Check for updates

Combining Nitrogen Isotopes and Redox Proxies Strengthens Paleoenvironmental Interpretations: Examples From Neoproterozoic Snowball Earth Sediments

Benjamin W. Johnson[1]*, Colin Mettam[2] and Simon W. Poulton[3]

[1]Earth System Evolution Laboratory, Iowa State University, Department of Geological and Atmospheric Sciences, Ames, IA, United States, [2]Department of Earth Sciences, University College London, London, United Kingdom, [3]School of Earth and Environment, University of Leeds, Leeds, United Kingdom

The history of the nitrogen cycle on Earth is linked to the redox evolution of the surface environment. Many nitrogen cycle fluxes are microbially mediated, and the particular fluxes operating at any given time in an ecosystem depend on the presence, absence or abundance of oxygen. However, interpreting this relationship is complicated as several isotopic fractionations associated with N-cycling are not diagnostic of a particular redox state. Thus, linking nitrogen isotopic analyses with redox-sensitive proxies is essential when interpretating past environments. Specifically, we use concentrations of U, V and Mo, along with Fe-speciation, to augment and contextualize nitrogen isotopic measurements. As an example, we consider samples from the Neoproterozoic Cryogenian period to suggest that there was oxygenated water, with associated aerobic N cycle fluxes. This interpretation is based on positive $\delta^{15}N$ values between 4 to $8^0/_{00}$, Fe-speciation data consistent with anoxic bottom water during the Snowball ocean and oxygenated after, and redox-sensitive trace metals indicative of oxic weathering and surface water. Typically, high $\delta^{15}N$ values are interpreted to reflect enhanced denitrification. We propose potential causes including a post-Snowball freshwater melt lid that suppressed deep water ventilation and that denitrification occurred more rapidly at high temperatures after the Snowball. These interpretations are buttressed by combined N isotope and redox analyses. This approach is especially useful during times of dynamic redox in the ocean-atmosphere system to interpret biologic isotopic signals.

Keywords: nitrogen, isotope, Neoproterozoic, redox, Snowball Earth

1 NITROGEN AND REDOX BIOGEOCHEMISTRY

Nitrogen is a key nutrient for life, a major component of the atmosphere, and tracks connections between the biosphere, atmosphere, and geosphere over long time scales (Zerkle and Mikhail, 2017). It is possible to investigate changes in the evolution and operation of the ancient nitrogen cycle via stable isotope geochemistry[1] as nitrogen undergoes a number of biologically mediated, redox sensitive transformations, each of which is associated with an isotopic fractionation (see Stüeken et al., 2016a).

Atmospheric N_2 enters the biosphere via nitrogen fixation by diazotrophic organisms. Such fixing splits the triple bond in N_2 using the nitrogenase enzyme. The most common enzyme (Fe - Mo nitrogenase) produces a minimal isotopic effect (Zhang et al., 2014). Nitrogen which is then remineralised from diazotrophic biomass can be stable and bioavailable in the environment as NH_4^+ or, in the presence of oxygen, is transformed by microbes to NO_3^- via nitrification. Nitrification has a significant isotopic effect, with product NO_3^- being enriched by 13 to $38^0/_{00}$ compared to substrate NH_4^+ (e.g., Casciotti et al., 2003, 2011). Typically, in modern oxygenated waters, nitrification is complete, such that all available NH_4^+ is converted, and thus there is no net isotopic effect recorded in the resultant NO_3^-.

Denitrification and anammox, which are microbially mediated respiration reactions that transform NO_3^- to N_2 (with minor N_2O), imparts a large net isotope effect where product N_2 is about $25^0/_{00}$ depleted compared to reactant NO_3^-. In the modern ocean, water column denitrification occurs primarily in oxygen minimum zones, but is only *partial* as the wider ocean is oxygenated, leaving a residual pool of NO_3^- with an average $\delta^{15}N$ of 5 to $7^0/_{00}$ (Sigman et al., 2009). By contrast, in modern marine sediments, there is no net isotopic effect on the bioavailable N pool, as here conversion to N_2 is quantitative (Sigman et al., 2009). The same isotopic pattern would result from anaerobic ammonium oxidation (anammox), especially in the geologic record (Brunner et al., 2013).

We can observe in modern oceans that sedimentary N-isotope values reflect the integrated signal of nitrogen cycling by organisms in the water column (Tesdal et al., 2013). However, interpretation of N-isotope values is complicated by the fact that fractionations produced by transitions between N compounds are not diagnostic (Busigny et al., 2013; Ader et al., 2014, 2016; Stüeken et al., 2016b). For example, a bulk ecosystem $\delta^{15}N$ value of $0^0/_{00}$ typically indicates anaerobic conditions (e.g., Garvin et al., 2009), but could also reflect quantitative nitrification without any denitrification. The latter case could occur in a completely aerobic environment, and thus the same bulk $\delta^{15}N$ value could be produced under completely opposite redox conditions in the water column. These issues are amplified in ancient sediments and rocks, since we cannot measure contemporaneous water conditions during sediment deposition.

In the Precambrian, most measured $\delta^{15}N$ values from sediments are positive (Stüeken et al., 2016a). During this time, anoxic water and potential oxyclines were more widespread. As a result there are multiple scenarios which could lead to positive $\delta^{15}N$ values. For example, in a study of the Archean Mount McRae Shale and Brockman Iron Formations Busigny et al. (2013) measured variable but consistently positive $\delta^{15}N$ values. Such positive values could reflect partial assimilation of NH_4^+ enriched in ^{15}N due to partial oxidation to NO_2^-. Such oxidation could occur in a fully anoxic water column via reactions with Fe or mediated biologically in local oxygen "oases" or in pervasively oxygenated shallow water (Busigny et al., 2013).

Previous nitrogen isotope studies of Neoproterozoic sedimentary rocks observed mostly positive $\delta^{15}N$ values (Ader et al., 2014; Wang et al., 2017; Stüeken et al., 2019a). Such values have mostly been interpreted to reflect an aerobic nitrogen cycle, due to the similarity of measured $\delta^{15}N$ to the modern ocean. As discussed, however, the relationship between N-isotopes as recorded in sediments and water column redox state is not straightforward. There are multiple potential environmental redox structures that can produce similar $\delta^{15}N$ values in sediments.

Thus, in order to interpret nitrogen isotope data it is essential to independently establish redox conditions in the depositional environment. This ideally includes both water column and sediment-water interface proxy data. Previous work has combined redox proxies with carbon isotopes (e.g., Kunzmann et al., 2015), and some have combined redox proxies with nitrogen isotopes (Quan et al., 2008, 2013; Zerkle et al., 2017; Stüeken et al., 2019b). This is crucial, given the strong connection between nitrogen cycling and oxygen. In this contribution, we combined redox proxies - redox sensitive trace elements and Fe-speciation - and nitrogen isotopes. Specifically, we apply this approach to sediments from the Neoproterozoic Snowball Earth ocean with new measurements from the Mineral Fork and Kelley Canyon Formations in Utah, United States. We further compare our results to previous data from the Ghaub Formation (Johnson et al., 2017b) and find that syn-glacial sediments have consistently positive $\delta^{15}N$ values which increase after the glaciation. Iron speciation suggests mostly anoxic bottom water during the glaciation and oxygenated bottom water after. Redox sensitive trace element concentrations suggest oxic weathering and an oxygenated upper water column throughout both the glaciation and afterwards. Combining all data, we suggest persistent oxygenated shallow water during Snowball glaciations which expands in depth after the glaciations. This finding supports previous interpretations of the Neoproterozoic ocean redox structure, and provides additional evidence for oxygenated water in the syn-glacial ocean.

2 GEOLOGIC SETTING AND SAMPLE DESCRIPTIONS

Samples presented in this study are from the Marinoan Ghaub Formation, Namibia (Johnson et al., 2017b) and the Mineral Fork

---

[1]Nitrogen isotopes are presented in delta notation (per mil, $^0/_{00}$), where

$$\delta^{15}N = \left[\frac{^{15}N/^{14}N_{\text{sample}} - ^{15}N/^{14}N_{\text{standard}}}{^{15}N/^{14}N_{\text{standard}}} \right] 1000 \qquad (1)$$

The standard for N isotopes is atmospheric N_2, which is set to $0^0/_{00}$ definition.

FIGURE 1 | Generalized map showing outcrop area of Neoproterozoic strata in Utah, United States. Map is after Crittenden et al. (1983) and (Young, 2002). Generalized cross section is shown, with detail of Mineral Fork Canyon showing sample locations. Photo **(A)** shows Kelley Canyon Formation, and **(B)** and **(C)** show outcrop photos from Mineral Fork Canyon. Samples were taken from finely laminated units away from draping, as seen in photo c.

Tillite and Kelley Canyon Formation, Utah, USA (**Figure 1**). Detailed description of the Ghaub samples are in Johnson et al. (2017b), but briefly these units are interpreted to be glacial outwash deposited below the ice-grounding line. The sequence was deposited during the Marinoan (~ 650 to 635 Ma), though exactly when during this interval is unclear. The sampled unit unconformably overlies the Naarchams Member, and conformably grades upwards into the overlying cap carbonate, the Keilberg Member. In detail, the Ghaub Formation is predominantly detrital carbonate (Hoffman, 2016), as the glaciers in this area were eroding an underlying carbonate platform. Specifically, samples were taken from the Fransfontein Homocline (Hoffman, 2011).

The Mineral Fork Formation is found in the central Wastach Range and on Antelope Island in Utah, United States. The unit comprises interbedded diamictites, sandstones and mudstones (Ojakangas and Matsch, 1980; Christie-Blick, 1982). The diamictite is typically massive, while the sandstone is subfeldspathic to quartzose, and includes laminated and cross-bedded facies; mudstones contain rare dropstones, several Fe-rich layers (Young, 2002), and carbonaceous layers with microfossils (Knoll et al., 1981). The unit is interpreted as having been deposited in a marginal marine setting, with dynamic glacial activity and periodic connection to the open ocean (Crittenden et al., 1983). Further, the overall geologic setting is consistent with a rifted margin creating accommodation space, but the depositional rate of the diamictite could have been more rapid than the accumulation of space due to tectonic activity (Hoffman P. F. et al., 2017). The relationship between glaciation, rifting, and deposition during the Sturtian in western North America may be complex (e.g., Kennedy and Eyles, 2021). We assume, however, for this study, that the Mineral Fork Formation is the result of glacial deposition in a marginal marine environment.

Age constraints are relatively poor. The Mineral Fork overlies the Big Cottonwood Formation, which is stratigraphically correlated with the ~ 766 Ma Uinta Mountain Group (Link and Christie-Blick, 2011). High Fe content supports association with Sturtian glaciation successions in North America (Young, 2002). The cap carbonate above the Mineral Fork Formation, however, is visually and texturally similar to the Keilberg Member in Namibia, supportive of a Marinoan age. Detrital zircons from the Kelley Canyon Formation yield maximum deposition ages for the till of 703 ± 6 Ma and an overlying graywacke of 667 ± 5 Ma (Balgord et al., 2013). There are no strong minimum age constraints. Thus, while existing geochronology does not rule out a younger, Marinoan age, these data more strongly support that the Mineral Fork tillite is Sturtian in age.

The paleogeographic location and tectonic setting of the Mineral Fork Formation is also not well constrained, due to its uncertain age. If the Mineral Fork is Sturtian, it is likely that it was deposited in a rift basin (Li et al., 2013; Merdith et al., 2017). Such a setting is more likely to have been a restricted basin, and thus would not record global oceanic geochemical conditions. If, however, the Mineral Fork is Marinoan, it was more likely deposited in a basin that was better connected to the global ocean (Li et al., 2013; Merdith et al., 2017). Regardless of this under-constrained geological setting, the main purpose of this study is to demonstrate that interpreting N isotopes in the geologic record is strengthened by combined consideration of independent redox proxies. Providing better constraints on the age of the Mineral Fork Formation, and whether or not these samples represent local or global signals, are beyond the scope of this paper.

We also analyzed samples from the Kelley Canyon Formation, which includes a post-Marinoan cap dolomite and a slate

TABLE 1 | Sample location and geologic information.

Sample	Latitude	Longitude	Formation	Lithology
BWJ18094	40° 36′ 59.8″	111° 40′ 45.3″	Mineral Fork	Massive till with cm clasts
BWJ18095	40° 36′ 39.9″	111° 40′ 46.2″	Mineral Fork	Coarse sandstone, cross-bedding
BWJ18096	40° 36′ 39.9″	111° 40′ 35.4″	Mineral Fork	Fine sandstone, ripple marks
BWJ18097	40° 36′ 39.9″	111° 40′ 35.4″	Mineral Fork	Fine grained sedimentary drape over dropstone
BWJ18098	40° 36′ 39.9″	111° 40′ 35.4″	Mineral Fork	Sandstone
BWJ18099	40° 36′ 39.9″	111° 40′ 35.4″	Mineral Fork	Fine grained black shale
BWJ18100	40° 36′ 39.9″	111° 40′ 35.4″	Mineral Fork	Fine grained black shale
BWJ18101	40° 36′ 39.9″	111° 40′ 35.4″	Mineral Fork	Fine grained black shale
BWJ18102	40° 59′ 1.62″	112° 12′ 49.32″	Kelley Canyon	Shale/slate, purple and resistant
BWJ18103	40° 59′ 1.62″	112° 12′ 49.32″	Kelley Canyon	Shale/slate, tan and resistant
BWJ18104	40° 59′ 1.62″	112° 12′ 49.32″	Kelley Canyon	Shale/slate, green-gray and recessive

member (**Table 1**). Specifically, samples are from the slate member and from three distinct facies. The three facies contain layers that are purple and resistant, tan and resistant, and green-gray recessive. Bedding in all facies is thin (~1–3 cm), supporting a depositional setting that is below wave-base (**Table 1**).

3 ANALYTIC TECHNIQUES

For all samples, we collected specimens free of obvious weathering or alteration. Prior to analyses, weathered edges of hand samples were trimmed with a rock saw. Samples were broken into smaller pieces with a rock hammer, and crushed to a powder in a motorized agate mortar and pestle. As detailed later, we argue that analyzed values represent primary values. Regional metamorphism was greenschist facies or lower (Yonkee et al., 2014), and measured values are very similar to previous work (Johnson et al., 2017b).

## 3.1 Nitrogen Concentration and Isotopes

Nitrogen isotopic techniques for the Namibian samples are presented in (Johnson et al., 2017b), and are similar for Mineral Fork and Kelley Canyon Formation samples. Nitrogen concentration and isotope ratios for the Mineral Fork Formation were characterized at the University of Colorado Boulder Earth Systems Stable Isotope Lab (CUBES-SIL), and values for the Kelley Canyon Formation were determined, using identical protocol, at the Earth System Evolution Lab (EaSEL) at Iowa State University. Carbon concentrations were obtained during the same runs as N concentration and isotopic analyses, using the same standards.

Sample powders were decarbonated via reaction with 5 ml of 6 N HCl. Samples were then sonicated for 30 min. All tubes were then placed in a 60°C oven overnight. The next day, samples were centrifuged to settle all undissolved material. Acid was poured off, fresh acid was added as before, and samples sat in the oven overnight. This acid refresh was repeated once more. To clean samples, all were rinsed three times with DI H_2O, centrifuging between each rinse. Sample powders then dried at 60°C for 2 days; all vials containing multiples of the same sample powder were combined and homogenized after drying.

Samples were then analyzed on a Thermo Delta V after combustion in a Thermo Elemental Analyzer at CUBES-SIL and on a Thermo Delta V Plus following combustion in a Thermo Isolink EA at EaSEL. Between 50 and 100 mg of sample powder was weighed into a Sn capsule, as well as standards: two acetanilides (act1, $\delta^{15}N = 1.18^0/_{00} \pm 0.02$ and act2, $\delta^{15}N = 19.56^0/_{00} \pm 0.03$) and pugel ($\delta^{15}N = 5.45^0/_{00} \pm 0.1$) at CUBES-SIL and urea (internal, $\delta^{15}N = -2.60 \pm 0.2^0/_{00}$) and caffeine (USGS62, $\delta^{15}N = 20.17 \pm 0.1^0/_{00}$) at EaSEL. All samples were flash-combusted with an excess of O_2 at 1,020°C in a combustion column packed with cobaltous oxide (combustion aid) and silvered cobaltous oxide (sulphur scrubber). Combustion products were passed over a reduced copper to reduce all N to N_2 and absorb excess O_2. Finally, sample gas was passed through a magnesium perchlorate trap to absorb water and a 3 m gas chromatography column to separate N_2 from CO_2. All analyses were quantified using IsoDat software and the Isoreader pipeline (Kopf et al., 2021). Errors reported are standard deviations from repeated analyses.

While the dominant mineralogy of the Ghaub at this location is carbonate, the geochemical results presented here, and in Johnson et al. (2017b), reflect analysis of the siliciclastic portion of the Ghaub sediment. Carbonate was removed via dissolution, so that the clay minerals could be analyzed directly. Clays record both the N signal (Ader et al., 2016) and the trace metal budget (Tribovillard et al., 2006; Johnson et al., 2017b).

Mineral Fork and Kelley Canyon samples were analyzed in the same run as previously measured glacial till samples (Timeball Hill and Blaubeker) from published work (Gaschnig et al., 2016; Johnson et al., 2017b). Measured N and $\delta^{15}N$ for Timeball (250 ppm, $5.06^0/_{00}$) and Blaubeker (158 ppm, $4.1^0/_{00}$) are similar to published values: 305 ± 5 ppm and $4.9 \pm 0.3^0/_{00}$ for Timeball Hill; and 90 ± 20 ppm and $4.4 \pm 0.2^0/_{00}$ for Blaubeker. We note that agreement in $\delta^{15}N$ values is quite good, though there are differences in N concentration outside uncertainty. Further, we also ensured that organic standards (urea, acetanilide, pugel, and caffeine) used to calculate N concentration included very small standard amounts (< 10 μg total mass) to capture relatively low N content in these rocks. The overall N concentrations are in the 100s of ppm, which is a
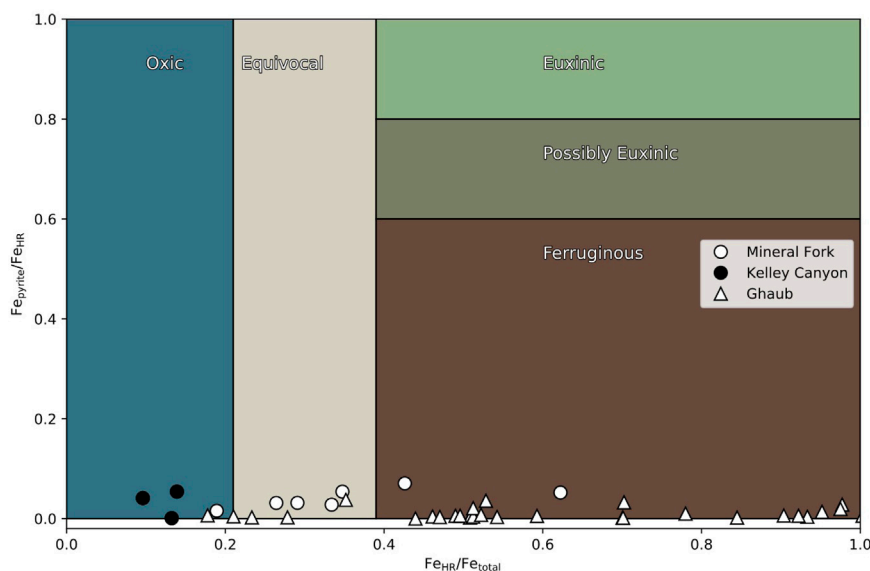
FIGURE 2 | Iron speciation data from the Mineral fork tillite (circles), Kelley Canyon Formation (filled circles) and the Ghaub Formation (triangles). Some samples from both settings plot in the fields characteristic of oxic bottom waters. Specifically, Kelley Canyon samples reflect oxic bottom waters with some samples from the Ghaub formation as well.

reasonable N content suitable for EA-IRMS analysis (Bräuer and Hahne, 2005; Boocock et al., 2020).

3.2 Redox Proxies

The Fe speciation method targets operationally defined Fe pools, including carbonate-associated Fe (Fe_{carb}), ferric oxide Fe (Fe_{ox}), magnetite Fe (Fe_{mag}) and pyrite Fe (Fe_{py}). Extractions were performed according to well-established protocols (Poulton and Canfield, 2005, 2011; Poulton, 2021), with subsequent analysis via atomic absorption spectroscopy (AAS) for Fe_{carb}, Fe_{ox} and Fe_{mag} at the University of Leeds. Fe_{py} was determined gravimetrically following chromous chloride distillation at the University of St Andrew's. Previous studies have shown reproducibility of better than ±2% (Mettam et al., 2017). Total Fe (Fe_T) was determined after HF–HClO$_4$–HNO$_3$ dissolution via AAS. All Fe extractions gave a relative standard deviation (RSD) of < 5% based on replicate analyses, and sequential extraction analyses were within 5% of the international Fe-speciation reference material WHIT (Alcott et al., 2020). Total dissolution of international sediment standards (USGS; SGR-1bl; USGS SBC-1) gave an Fe recovery of > 98%.

The sum of Fe_{carb}, Fe_{ox}, Fe_{mag} and Fe_{py} defines a highly reactive (Fe_{HR}) pool, which is considered to represent Fe that is biogeochemically reactive during deposition and early diagenesis (Raiswell and Canfield, 1998; Poulton et al., 2004). Anoxic waters commonly have Fe_{HR}/Fe_T ratios > 0.38, in contrast to oxic depositional conditions where ratios are generally < 0.22 (Poulton and Canfield, 2011). Elevated Fe_{HR}/Fe_T ratios in anoxic settings arise from the additional water column formation of pyrite in euxinic (sulphidic) settings, or unsulphidized Fe_{HR} minerals in ferruginous (Fe-containing) settings. Thus, for anoxic samples (i.e., Fe_{HR}/Fe_T > 0.38) the

ratio of Fe_{py}/Fe_{HR} distinguishes euxinic (Fe_{py}/Fe_{HR} > 0.8) from ferruginous (Fe_{py}/Fe_{FR} < 0.6) water column conditions (Poulton and Canfield, 2011; Benkovitz et al., 2020; Poulton, 2021). Fe_{HR}/Fe_T ratios of 0.22–0.38 are considered equivocal, and may occur due to the masking of water column enrichments via rapid sedimentation (e.g., during turbidite deposition Canfield et al., 1996), or due to transformation of unsulphidized Fe_{HR} to clay minerals during diagenesis and metamorphism (e.g., Poulton et al., 2010). This second possibility can be evaluated by considering Fe/Al ratios, since Fe_T is preserved even if Fe_{HR} is lost to clay minerals. In this case, normal oxic marine shales tend to have Fe/Al ratios of 0.55 ± 0.11, and thus Fe/Al > 0.66 is considered to provide a robust indication of water column anoxia (Clarkson et al., 2014).

Trace element composition was determined by ActLabs following their Ultratrace 4 protocol (https://actlabs.com/geochemistry/exploration-geochemistry/4-acid-near-total-digestion/). This is a total digestion using HF, HNO$_3$ and HCl, followed by analysis via ICP-MS. All measured values are above stated detection limits which are 0.1, 1 and 0.05 ppm for U, V and Mo, respectively. Reported accuracy for all elements are within 1–5% compared to certified standards (GXR-4, SDC-1, DNC-1a, and SBC-1). Reported precisions are ±0.3 ppm for U, ± 2 ppm for V, and ±0.1 ppm for Mo.

4 RESULTS AND INTERPRETATION

We will first discuss the Fe-speciation and U, V and Mo redox proxy data. These establish the geochemical boundary conditions that govern the nitrogen cycle, and within which N isotope data can be interpreted. Then, we place the N isotopic data within this

TABLE 2 | Geochemical data presented in text. Nitrogen and trace element concentrations are given in ppm, while Al and Fe speciation data are in weight percent. Nitrogen isotope values are in permil (%), compared to atmospheric N_2.

Sample name	N	$\delta^{15}N$	V	Mo	U	Zr	Al	Fe_{carb}	Fe_{ox}	Fe_{mag}	Fe_{pyrite}	Fe_{total}	Fe/Al
BWJ18094	212	4.1	56.0	0.2	1.4	38.0	4.36						
BWJ18095	130		20.0	0.2	0.4	20.0	1.89	0.10	0.56	0.03	0.04	1.17	0.62
BWJ18096	220	7.7	64.0	4.8	1.9	69.0	5.41	1.58	0.55	0.84	0.23	7.50	1.39
BWJ18097	353	7.6	56.0	0.1	3.2	57.0	7.69	0.35	0.86	0.22	0.08	4.35	0.57
BWJ18098	302	7.0	72.0	0.2	3.6	91.0	8.50	0.50	0.40	0.61	0.02	8.11	0.95
BWJ18099	326	6.2	34.0	0.0	2.9	55.0	7.62	0.29	0.60	0.29	0.04	4.19	0.55
BWJ18100	402	6.8	67.0	0.1	2.5	57.0	8.11	0.20	0.64	0.25	0.04	4.26	0.53
BWJ18101	393	4.8	42.0	0.0	2.8	66.0	8.94	0.21	0.87	0.16	0.04	3.82	0.43
BWJ18102	166	6.7	56.0	0.1	6.0	74.0	10.00	0.06	0.85	0.16	0.00	8.09	0.81
BWJ18103	101	8.2	25.0	0.0	4.4	134.0	7.62	0.22	0.05	0.01	0.02	2.13	0.28
BWJ18104	118	8.9	50.0	0.1	4.8	161.0	9.64	0.05	0.16	0.00	0.01	2.28	0.24
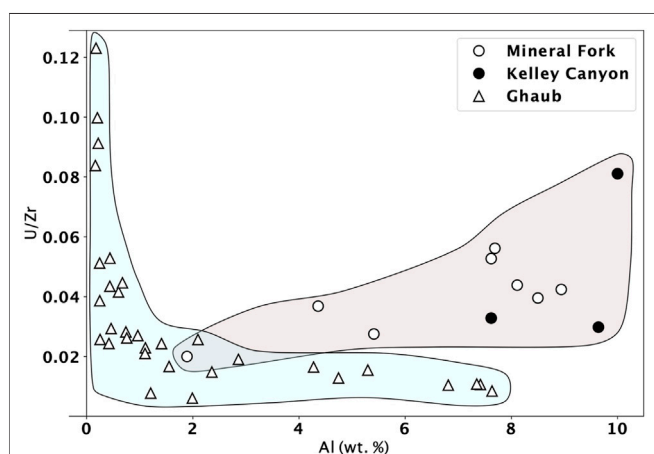
FIGURE 3 | U/Zr ratio from the Mineral fork tillite (circles) and the Ghaub Formation (triangles) plotted against Al concentration. Uranium and Zr are similar geochemically, except U is redox sensitive and Zr is not. Therefore, correlation of this ratio with Al, a proxy for detrital influence, can distinguish between changing U concentrations caused by detrital input or redox evolution. We suggest that only moderate control of U concentration by detrital input is evident in samples from Utah (Mineral Fork and Kelley Canyon). In contrast, Ghaub samples show authigenic enrichment in U, with high U at low Al content. Ghaub and Utah samples show a distinct trend, highlighted by the blue and peach fields.

geochemical context. We also include data from Johnson et al. (2017b).

4.1 Redox Proxies

Iron speciation data from the Ghaub Formation are characteristic of anoxic, ferruginous bottom water (**Figure 2**), with Fe_{pyrite}/Fe_{HR} ratios below 0.1 and Fe_{HR}/Fe_{total} above 0.38. The Mineral fork and Kelly Canyon Formations, however, have Fe speciation data ranging from ferruginous to oxic conditions. In both Utah and Namibia, there appears to be minor fluctuations between anoxic and possibly oxic conditions, but in the samples from the Kelley Canyon Formation reflect oxygenated bottom waters after the Snowball glaciation (**Table 2**).

In all Utah samples, Mo is low, between detection limit of 0.05 ppm and 0.24 ppm, with the exception of one sample at 4.8 ppm.

Vanadium ranges from 20–72 ppm, and U ranges from 0.4 to 6 ppm, with most values above 2.5 ppm (**Table 2**). These variations are only partially due to differential detrital input, as seen by plotting U normalized to Zr as a function of Al (**Figure 3**). Zirconium is geochemically similar to U, but Zr is non redox-active, and when plotted against Al (a proxy for detrital input), it is apparent that there is a weak correlation ($r^2 = 0.36$). This indicates that some variation in trace metal abundance may be related to detrital input into the basin, but it is likely not the primary control. In contrast, we observe high U values at low Al concentration in Ghaub samples, indicating authigenic enrichment of U in this location.

There is no clear correlation, however, between the trace element concentration (U and Mo), normalized to Post-Archean Average Shale (PAAS), and total organic carbon (TOC) (**Figure 4**). By normalizing to PAAS, we are showing whether or not each trace element is enriched compared to the average over time. Such an "enrichment factor", when plotted as a function of TOC, is an effective redox proxy (Algeo and Liu, 2020). Specifically, this indicates that scavenging by organic carbon during burial is unlikely to be the primary control on trace element abundance. Rather, the abundance of trace elements indicate oxic weathering and delivery of soluble forms of these elements to the water column.

Johnson et al. (2017b) interpreted the Mo, U and V data from Namibia to reflect oxic weathering on the continents, followed by delivery to the ocean and scavenging in ferruginous bottom waters. While U supply is controlled by detrital input, by normalizing to Al (**Figure 3**), Johnson et al. (2017b) demonstrated that changing U concentrations were not due to changing detrital input alone, and were consistent with iron speciation data. Similarly, these redox-sensitive elements from Utah are present in similar concentrations (**Figure 5**). Uranium, specifically, also displays a negative correlation with Fe_{HR}/Fe_{Total}, consistent with higher U concentrations reflecting a more pervasively oxygenated water column.

There is no enrichment, however, in Mo or V observed from the Mineral Fork or Kelley Canyon formation. Recent work from the early Cambrian of South China has suggested that in settings with a well developed, dynamic redox-cline, the behavior of Mo, V, and U may be decoupled (Han et al., 2018). Specifically, the
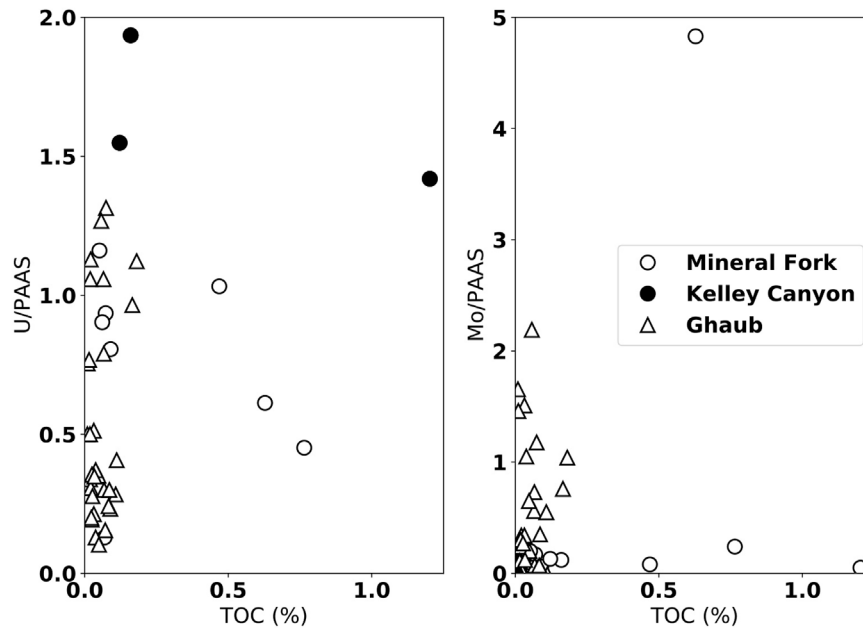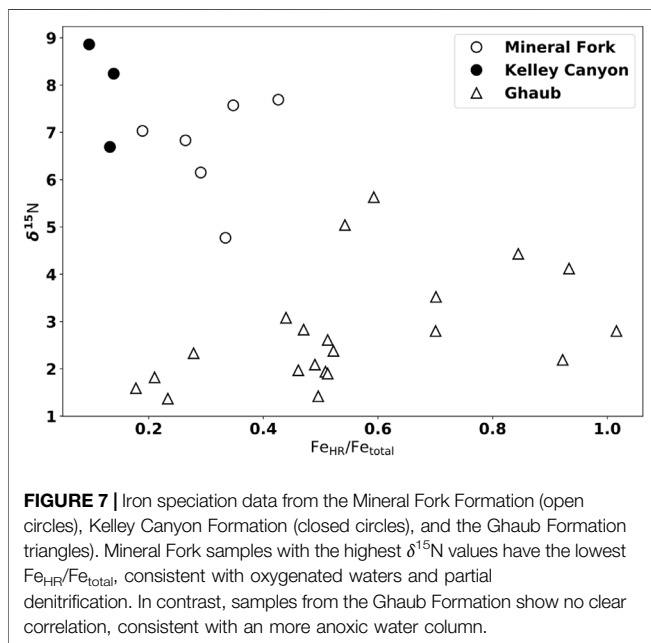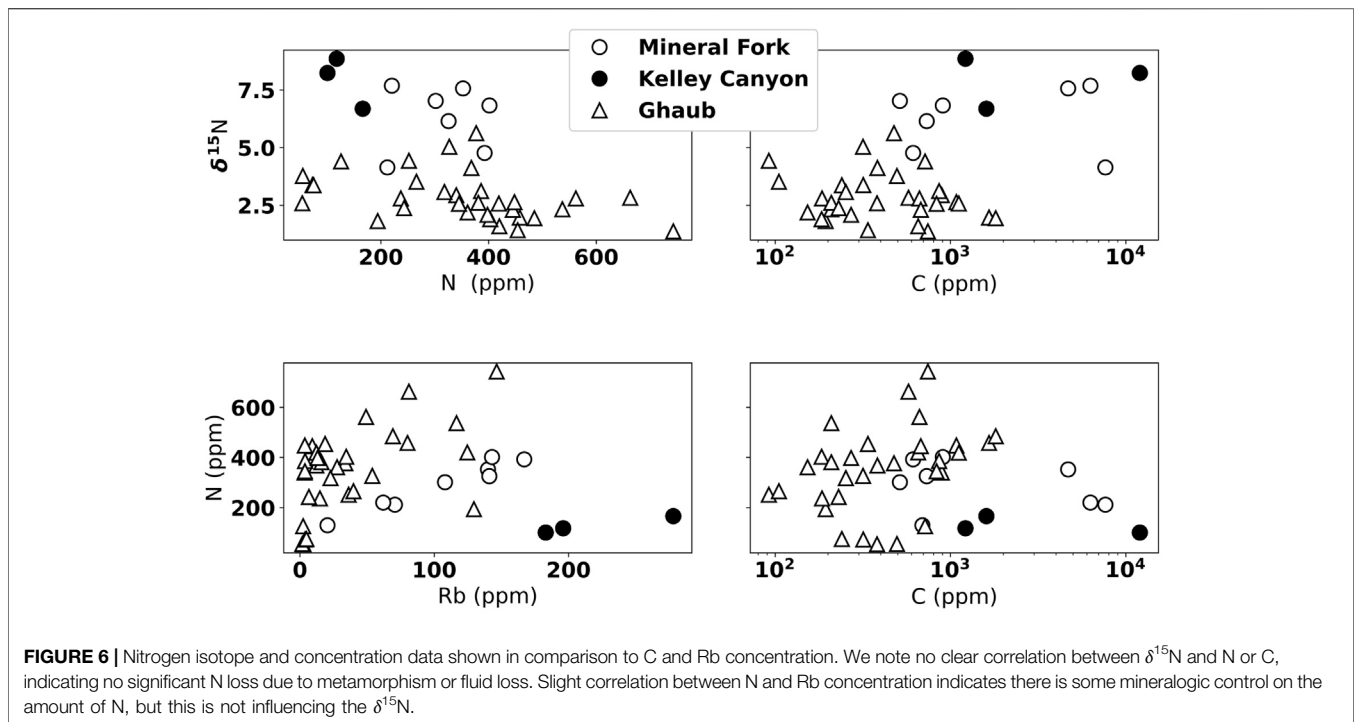
FIGURE 4 | Uranium and Mo concentrations, normalized to Post-Archean Average Shale (PAAS), plotted against carbon concentration (ppm) from the Mineral fork (open circles), Kelley Canyon (closed circles), and the Ghaub Formation (triangles). There is no clear correlation between either, suggesting limited influence of organic carbon availability on trace metal concentration in sediments.
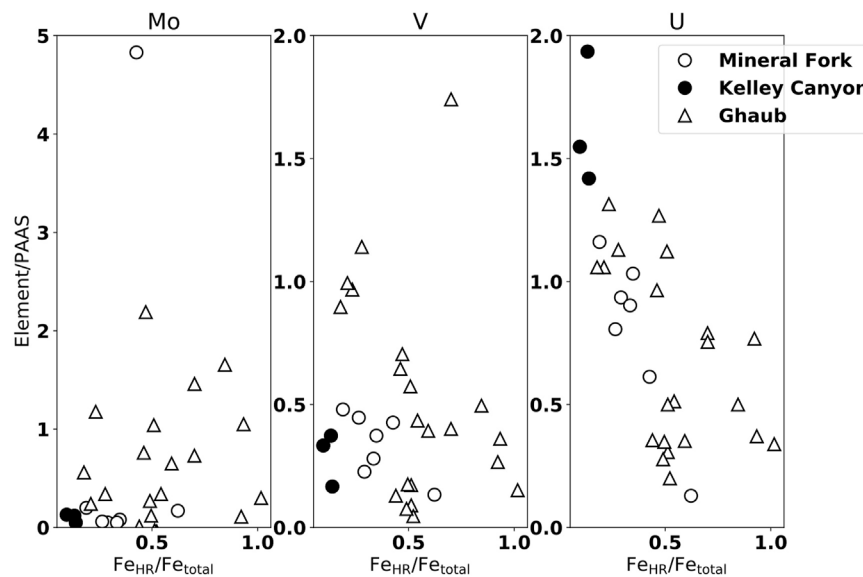
FIGURE 5 | Trace element concentrations normalized to Post-Archean Average Shale (PAAS), plotted against iron speciation data from the Mineral Fork (open circles), Kelley Canyon (closed circles), and the Ghaub Formation (triangles). In general, the Ghaub Formation has higher enrichments in all redox sensitive trace elements, but values above one indicate oxic weathering of continental crust (e.g., Algeo and Tribovillard, 2009; Johnson et al., 2017b). Uranium is enriched relative to PAAS in the samples from Utah, while V and Mo are not.

presence of a zone of Fe-Mn particulate formation can preferentially enrich sediments in V. If such a zone is absent, or sediments sampled are from shallower water, such V

enrichment could be missing. It is likely that the Mineral Fork samples were deposited near the ice-grounding line (Christie-Blick, 1982), and perhaps the water column at this location did

FIGURE 6 | Nitrogen isotope and concentration data shown in comparison to C and Rb concentration. We note no clear correlation between δ^{15}N and N or C, indicating no significant N loss due to metamorphism or fluid loss. Slight correlation between N and Rb concentration indicates there is some mineralogic control on the amount of N, but this is not influencing the δ^{15}N.

FIGURE 7 | Iron speciation data from the Mineral Fork Formation (open circles), Kelley Canyon Formation (closed circles), and the Ghaub Formation triangles). Mineral Fork samples with the highest δ^{15}N values have the lowest Fe_{HR}/Fe_{total}, consistent with oxygenated waters and partial denitrification. In contrast, samples from the Ghaub Formation show no clear correlation, consistent with an more anoxic water column.

not contain a Fe-Mn particulate shuttle, leading to low V concentrations.

Overall concentrations of these elements observed from Utah and Namibia are similar to other work focused on the Cryogenian. For example, a section spanning both Sturtian and Marinoan from the Zavkhan Terrane, southwest Mongolia finds U concentrations of between 0.05 and 2 ppm, very similar to our measurements (Lau et al., 2017). Trace element

measurements from the Doushantuo Formation of South China, deposited after the Marinoan glacial period, display quite high concentrations of U (up to 30 ppm), V (1,000 ppm), and Mo (200 ppm) in the immediate deglacial period, with values decreasing rapidly up-section (Sahoo et al., 2012). Since the Kelley Canyon formation overlies the cap carbonate, it would have been deposited sometime after the deglaciation, and thus likely does not capture the immediate deglaciation.

4.2 Nitrogen Isotopes

We present N concentration and isotope data in **Figure 6**. δ^{15}N in both Namibia and Utah are positive, between about 1 to $5^0/_{00}$ from the Ghaub and 4.1 to $7.6^0/_{00}$ in the Mineral Fork (**Figures 6, 7**). Values from the Kelley Canyon Formation are higher, between 6.7 to $8.9^0/_{00}$. Nitrogen concentration is similar in units from Namibia and Utah, ranging from 100 to 650 ppm. As noted in **Section 3.1**, analysis of previously measured till samples from the Timeball Hill and Blaubeker formations produced nearly identical δ^{15}N values but different N concentrations. Previous work has noted that within-sample heterogeneity may be an issue for N measurements (Johnson et al., 2017a). Rock hosted N can potentially exist as different species (e.g., NH_4^+, NO_3^-, N_2) and in different organic or mineral phases. So, it is possible that small scale heterogeneity, or slightly different analytical conditions/ techniques may be liberating different pools of N. Bulk N isotope values, however, seem to be robust even if measured N concentrations vary (Bräuer and Hahne, 2005; Boocock et al., 2020).

To assess the potential influence of metamorphic alteration of N content and isotopic signals, we show δ^{15}N plotted against

N concentration, Rb concentration, and C concentration (**Figure 6**). We observe no correlation between $\delta^{15}N$ and N concentration, suggesting that higher $\delta^{15}N$ values are not caused by progressive N loss during metamorphism (Bebout and Fogel, 1992). There is a rough correlation between N and Rb concentration, suggesting some variation in N content could be related to detrital input. The lack of correlation, however, between $\delta^{15}N$ and N concentration again indicates that while there might be some lithologic control on total N, this does not influence isotope values. There is not a clear correlation between C and N content, which is different than previous work on the non-glacial Neoproterozoic (e.g., Ader et al., 2014), but similar to previous analyses of syn-glacial units (Johnson et al., 2017b). This suggests that there may be either differential preservation of N and C in these units, or that the N and C cycles are differently coupled during Snowball glaciations than the non-glacial intervals of the Cryogenian.

Assuming atmospheric N_2 was at $0^0/_{00}$ during the Cryogenian (Stüeken et al., 2016b), enriched $\delta^{15}N$ values, given the evidence of persistent O_2 availability provided by redox-sensitive element data, are consistent with the presence of partial, water-column denitrification during the Snowball glaciation. That is, there must have been sufficient O_2 present to support nitrification, with denitrification occurring at boundaries between oxygenated and low-oxygen waters, with a likely chemocline location in bottom waters. The similarity of Mineral Fork $\delta^{15}N$ values to average modern marine values (5 to $7^0/_{00}$) indicates that a similar relative amount of partial denitrification ($\sim 20\%$) was occurring in the water column (Tesdal et al., 2013).

After the glaciation, as preserved by the Kelley Canyon formation, samples have the highest $\delta^{15}N$ values measured. These values are typically interpreted to indicate more extensive denitrification, and lower water-column O_2, to drive residual N to higher $\delta^{15}N$ values. Yet, Fe-speciation data indicates oxygenated bottom waters during the deposition of the Kelley Canyon Formation (**Figures 2, 7**). Kelley Canyon units also have the highest U concentrations of any samples presented (**Figure 5**), suggesting oxic weathering and delivery of U to the site of deposition. Thus, we require an interpretation that can explain both higher $\delta^{15}N$ values and a pervasively oxygenated water column. We propose two potential explanations: oceanographic circulation shifts and biologic responses to deglaciation.

A similar pattern, positive but low and then increasing several permil, in $\delta^{15}N$ values in sediments has been observed in a number of locations during the Pleistocene-Holocene deglaciation (Galbraith and Kienast, 2013). Several sites are near-shore environments, including one off the coast of northern Chile (De Pol-Holz et al., 2006). De Pol-Holz et al. (2006) observed an increase in sedimentary $\delta^{15}N$ values from 8 to $12^0/_{00}$ across the deglaciation, and attributed this increase to melting of the Patagonian Ice Sheet. The influx of freshwater slowed formation of intermediate water, which in turn decreased deep water ventilation. This oceanographic reorganization could have resulted in upwelled N that was enriched in ^{15}N, due to removal by denitrification, compared to the glacial maximum with a less well developed oxygen

minimum zone. The Snowball deglaciation would have produced a large meltwater lid (Hoffman PF. et al., 2017), which could affect ocean circulation in a similar way: limited deep-water ventilation, increased denitrification at a chemocline underlying a well oxygenated upper water column.

In the wake of both the Sturtian and the Marinoan glaciations, the ocean appears to have become more oxygen rich and the surface temperature increased (Hoffman PF. et al., 2017; Lechte et al., 2019). There are many studies on contemporary denitrifying bacteria, both in the field and in culture, that demonstrate an increase in denitrification activity at higher temperatures (Nowicki, 1994; Veraart et al., 2011). Thus, we would expect to observe an increase in $\delta^{15}N$ in post-Snowball warm oceans, observed in both the Ghaub and Mineral Fork-Kelley Canyon Formations. While an increase in water column oxygen may seem anathema to increased denitrification, modern denitrifiers do function in oxygenated water. Specifically, by using the Nap reductase enzyme, instead of the Nar enzyme (Berks et al., 2001), organisms can perform aerobic denitrification (Ji et al., 2015). Perhaps, then, the combined effect of high temperatures and aerobic denitrification caused an increase in $\delta^{15}N$ values in the post-Snowball ocean, even in the presence of higher water column O_2.

Alternately, it is possible that enriched $\delta^{15}N$ values could reflect partial nitrification followed by complete denitrification. This scenario was proposed to explain very positive $\delta^{15}N$ values from the 2.7 Ga Tumbiana Formation (Thomazo et al., 2011), though an alternate explanation has been proposed suggesting high values could be caused by alkaline conditions and degassing of NH_3 (Stüeken et al., 2015). Nitrification to nitrite has a pronounced isotopic effect, with product NO_2^- depleted between 13 to $38^0/_{00}$ compared to reactant NH_4^+ (Casciotti et al., 2003). If, then, NO_2^- is quantitatively removed via anammox, the residual N pool would be comprised of isotopically enriched NH_4^+. In the modern ocean, this scenario has been observed in sediments of the Bering Sea (e.g., Morales et al., 2014). There is, however, a much wider range in sediment $\delta^{15}N$ values ($+2^0/_{00}$ to $+18^0/_{00}$), reflecting the transient nature of the geochemical conditions necessary for this to occur. Since the N isotope data from both Cryogenian sections are more tightly coupled with evidence for persistent oxic weathering, we suggest that they instead reflect less transient redox conditions, and likely complete nitrification followed by partial denitrification.

Additionally, we note that $\delta^{15}N$ values are generally lower in samples with Fe_{HR}/Fe_{total} values that are 'equivocal' compared to those that clearly plot in the ferruginous field (**Figure 2, 7**). Since this potential trend is not strongly correlated ($r^2 = 0.13$), any interpretations at this point are speculative. It is possible that samples with low Fe_{total}, and therefore higher Fe_{HR}/Fe_{total}, represent upwelling into oxygenated conditions, driving denitrification and increasing $\delta^{15}N$ values. However, iron speciation data does not allow for quantitative interpretation of bottom water conditions within fields, but rather serves to distinguish between overarching redox conditions. Future work, either observational or geochemical modeling, could be valuable to investigate any controls on patterns within Fe-speciation fields.

5 IMPLICATIONS FOR SNOWBALL OCEAN AND REDOX-BIOLOGIC INTERPRETATIONS

There are two major implications from this work. First, we present further support for periods of oxygenated water during the Snowball Earth glaciations based on Fe-speciation, redox sensitive trace elements and enriched $\delta^{15}N$ values. Second, we suggest corroborating evidence for a relatively rapid increase in oxygen content in the post-Snowball ocean set against a background of variable redox conditions (Kunzmann et al., 2017; Lau et al., 2017) while also providing hypotheses to explain positive $\delta^{15}N$ during the Snowball ocean that increased after the glaciation.

Previous data from Namibia, combining N isotopes and redox proxies, had suggested pockets of oxygenated water with active photosynthesis and aerobic N cycling during the Marinoan (Johnson et al., 2017b). Our work herein records similar geochemical values, consistent with a similar water-column redox/nutrient state. Thus, in at least two locations - during a Snowball ocean - there is geochemical evidence for oxygenated water. What is unclear, though, is whether samples from Namibia and Utah represent contemporaneous time periods. Age control from Namibia is relatively tight (Hoffman et al., 2021), clearly indicating the Ghaub Formation is Marinoan in age.

As previously mentioned, the age of the Mineral Fork is crucial for any interpretation linking this site to broader global patterns of redox structure. If the Mineral Fork is Sturtian, it is likely that it was deposited in a rifting basin (e.g., Balgord et al., 2013). The similarity of N and redox geochemical values from Mineral Fork and the Ghaub suggest that they record broadly similar ocean conditions. We cannot say to what extent this might be a global signal during each glaciation, since at present these are the only sites with N and redox data synchronous with the Snowball ocean. Perhaps, then, marginal marine settings during the Marinoan and Sturtian glaciations were geochemically similar. While it is beyond the scope of this paper to determine global ocean redox, our work does demonstrate that combining proxies from geographically distributed samples can help fill in this picture. We suggest long-lived open water and/or ample photosynthesis to keep the atmosphere and at least parts of the upper ocean oxygenated. There may even have been periodic bottom water oxygenation during the deposition of the Mineral Fork Formation.

Comparison to other geochemical and observational work also indicates the presence of persistent oxygenated environments throughout the Snowball ocean. For example, geochemical analyses of iron formations (IFs) indicate that subglacial meltwater would have provided O_2 to marginal marine settings (Lechte et al., 2019). Measurements of cyclicity in banded IFs are consistent with ice sheets responding dynamically to orbital forcing (Mitchell et al., 2021). A potential consequence of such orbital forcing is that dynamic ice could have facilitated oxygenation of the surface ocean via air-sea gas exchange upon either ice retreat or advancement (Mitchell et al., 2021).

Our work demonstrates the utility of the combined redox proxy-N isotope analytical strategy for characterizing Precambrian units. This is especially useful during times of dynamic fluctuations in oxygen, both in the atmosphere and ocean (Sperling et al., 2015; Wei et al., 2021). For example, previous work has demonstrated that different oceanic redox structures can result in similar ranges of $\delta^{15}N$ values recorded in sediment (Ader et al., 2014). Values above approximately $0^0/_{00}$ could be generated in the water column, and therefore recorded in sediments, either from modern-like conditions or strongly redox stratified conditions. For the former, this is the result of complete nitrification followed by partial denitrification. For the latter, higher than zero $\delta^{15}N$ values can be caused by a combination of ammonification and partial assimilation (Ader et al., 2014). Such a redox-cline can either be shallow or deep, and still produce similar $\delta^{15}N$ values.

Thus, water column redox reconstructions are crucial for interpretation of N isotopes. Specifically, using Fe-speciation for bottom water redox and redox-sensitive trace elements for surface water/atmospheric redox conditions can contextualize N isotopes values. As more work utilizes N isotope measurements as a tool to investigate both biologic and redox activity (e.g., Peng et al., 2020), placing such biologically controlled signals into a redox context will be crucial.

6 CONCLUSION

The evolution of ocean redox and water column nutrient cycling are closely intertwined over Earth history. There are a number of redox proxies, including redox sensitive trace metal abundance and iron speciation, that can be used to investigate oxygenation of the ancient atmosphere and oceans. Stable isotope ratios of major nutrients, such as carbon and nitrogen, are often used to reconstruct ancient microbial ecosystems and metabolisms. Nitrogen isotopes are commonly measured in ancient sediments, but produce non-diagnostic signals. Indeed, there is more than one pathway or combination of fluxes in the nitrogen cycle that could produce the same bulk $\delta^{15}N$ signal. Due to the tight relationship between the nitrogen cycle and oxygen availability, combining redox proxies with isotopic measurements provides insight and context into the redox environment crucial for interpreting isotopic signals.

We utilized a combined redox and N-isotope approach to specifically highlight the nitrogen cycle during the Neoproterozoic Snowball Earth glaciations. We analyzed deposits from Utah, USA likely preserving the Sturtian (Mineral Fork Formation) and post-Sturtian (Kelley Canyon Formation) time periods, and show previous work from the Ghaub Formation in Namibia for comparison (Johnson et al., 2017b). We find that redox proxies (U, V and Mo concentrations, and Fe speciation) are consistent with the presence of oxygenated water near the surface and potentially near the sediment water interface as well. Nitrogen isotope ratios are all above $0^0/_{00}$,

and given redox constraints, are indicative of nitrification followed by partial denitrification in the water column. The geochemical proxies are quite similar between the two field sites, suggesting similar water conditions at different paleogeographic locations and times. That is, we present evidence for oxygenated water during Cryogenian glaciations. More broadly, our work shows that combining these two approaches yields a deeper insight into ancient ecosystems and water conditions over Earth history. We also highlight the importance of considering oceanographic and biologic interpretations of redox data, as these are important factors controlling N isotope signals in biomass and sediments through time.

DATA AVAILABILITY STATEMENT

The original contributions presented in the study are included in the article/**Supplementary Materials**, further inquiries can be directed to the corresponding author.

REFERENCES

AUTHOR CONTRIBUTIONS

BJ designed the study, collected the samples, conducted N isotopic measurements, interpreted results, and prepared the manuscript. SP conducted Fe-speciation work, interpreted results, and prepared the manuscrpit. CM conducted Fe-speciation work, interpreted results, and prepared the manuscript.

SUPPLEMENTARY MATERIAL

The Supplementary Material for this article can be found online at: https://www.frontiersin.org/articles/10.3389/feart.2022.745830/full#supplementary-material

Ader, M., Sansjofre, P., Halverson, G. P., Busigny, V., Trindade, R. I. F., Kunzmann, M., et al. (2014). Ocean Redox Structure across the Late Neoproterozoic Oxygenation Event: a Nitrogen Isotope Perspective. *Earth Planet. Sci. Lett.* 396, 1–13. doi:10.1016/j.epsl.2014.03.042

Ader, M., Thomazo, C., Sansjofre, P., Busigny, V., Papineau, D., Laffont, R., et al. (2016). Interpretation of the Nitrogen Isotopic Composition of Precambrian Sedimentary Rocks: Assumptions and Perspectives. *Chem. Geol.* 429, 93–110. doi:10.1016/j.chemgeo.2016.02.010

Alcott, L. J., Krause, A. J., Hammarlund, E. U., Bjerrum, C. J., Scholz, F., Xiong, Y., et al. (2020). Development of Iron Speciation Reference Materials for Palaeoredox Analysis. *Geostand. Geoanal Res.* 44, 581–591. doi:10.1111/ggr.12342

Algeo, T. J., and Liu, J. (2020). A Re-assessment of Elemental Proxies for Paleoredox Analysis. *Chem. Geol.* 540, 119549. doi:10.1016/j.chemgeo.2020.119549

Algeo, T. J., and Tribovillard, N. (2009). Environmental Analysis of Paleoceanographic Systems Based on Molybdenum-Uranium Covariation. *Chem. Geol.* 268, 211–225. doi:10.1016/j.chemgeo.2009.09.001

Balgord, E. A., Yonkee, W. A., Link, P. K., and Fanning, C. M. (2013). Stratigraphic, Geochronologic, and Geochemical Record of the Cryogenian Perry Canyon Formation, Northern Utah: Implications for Rodinia Rifting and Snowball Earth Glaciation. *Geol. Soc. Am. Bull.* 125, 1442–1467. doi:10.1130/b30860.1

Bebout, G. E., and Fogel, M. L. (1992). Nitrogen-isotope Compositions of Metasedimentary Rocks in the Catalina Schist, California: Implications for Metamorphic Devolatilization History. *Geochimica Cosmochimica Acta* 56, 2839–2849. doi:10.1016/0016-7037(92)90363-N

Benkovitz, A., Matthews, A., Teutsch, N., Poulton, S. W., Bar-Matthews, M., and Almogi-Labin, A. (2020). Tracing Water Column Euxinia in Eastern Mediterranean Sapropels S5 and S7. *Chem. Geol.* 545, 119627. doi:10.1016/j.chemgeo.2020.119627

Boocock, T. J., Mikhail, S., Prytulak, J., Di Rocco, T., and Stüeken, E. E. (2020). Nitrogen Mass Fraction and Stable Isotope Ratios for Fourteen Geological Reference Materials: Evaluating the Applicability of Elemental Analyser versus Sealed Tube Combustion Methods. *Geostand. Geoanal Res.* 44, 537–551. doi:10.1111/ggr.12345

Bräuer, K., and Hahne, K. (2005). Methodical Aspects of the 15N-Analysis of Precambrian and Palaeozoic Sediments Rich in Organic Matter. *Chem. Geol.* 218, 361–368. doi:10.1016/j.chemgeo.2005.01.004

Brunner, B., Contreras, S., Lehmann, M. F., Matantseva, O., Rollog, M., Kalvelage, T., et al. (2013). Nitrogen Isotope Effects Induced by Anammox Bacteria. *Proc. Natl. Acad. Sci. U.S.A.* 110, 18994–18999. doi:10.1073/pnas.1310488110

Busigny, V., Lebeau, O., Ader, M., Krapež, B., and Bekker, A. (2013). Nitrogen Cycle in the Late Archean Ferruginous Ocean. *Chem. Geol.* 362, 115–130. doi:10.1016/j.chemgeo.2013.06.023

Canfield, D. E., Lyons, T. W., and Raiswell, R. (1996). A Model for Iron Deposition to Euxinic Black Sea Sediments. *Am. J. Sci.* 296, 818–834. doi:10.2475/ajs.296.7.818

Casciotti, K. L., Buchwald, C., Santoro, A. E., and Frame, C. (2011). Assessment of Nitrogen and Oxygen Isotopic Fractionation during Nitrification and its Expression in the Marine Environment. *Methods Enzym. (Elsevier)* 486, 253–280. doi:10.1016/b978-0-12-381294-0.00011-0

Casciotti, K. L., Sigman, D. M., and Ward, B. B. (2003). Linking Diversity and Stable Isotope Fractionation in Ammonia-Oxidizing Bacteria. *Geomicrobiol. J.* 20, 335–353. doi:10.1080/01490450303895

Christie-Blick, N. (1982). Upper Proterozoic and Lower Cambrian Rocks of the Sheeprock Mountains, Utah: Regional Correlation and Significance. *Geol. Soc. Am. Bull.* 93, 735–750. doi:10.1130/0016-7606(1982)93<735:upalcr>2.0.co;2

Clarkson, M. O., Poulton, S. W., Guilbaud, R., and Wood, R. A. (2014). Assessing the Utility of Fe/Al and Fe-Speciation to Record Water Column Redox Conditions in Carbonate-Rich Sediments. *Chem. Geol.* 382, 111–122. doi:10.1016/j.chemgeo.2014.05.031

Crittenden, M. D., Jr, Christie-buck, N., and Karl Link, P. (1983). Evidence for Two Pulses of Glaciation during the Late Proterozoic in Northern Utah and Southeastern Idaho. *Geol. Soc. Am. Bull.* 94, 437–450. doi:10.1130/0016-7606(1983)94<437:eftpog>2.0.co;2

De Pol-Holz, R., Ulloa, O., Dezileau, L., Kaiser, J., Lamy, F., and Hebbeln, D. (2006). Melting of the Patagonian Ice Sheet and Deglacial Perturbations of the Nitrogen Cycle in the Eastern South Pacific. *Geophys. Res. Lett.* 33, 24477. doi:10.1029/2005gl024477

Galbraith, E. D., Kienast, M., and Kienast, M. (2013). The Acceleration of Oceanic Denitrification during Deglacial Warming. *Nat. Geosci.* 6, 579–584. doi:10.1038/ngeo1832

Garvin, J., Buick, R., Anbar, A. D., Arnold, G. L., and Kaufman, A. J. (2009). Isotopic Evidence for an Aerobic Nitrogen Cycle in the Latest Archean. *Science* 323, 1045–1048. doi:10.1126/science.1165675

Gaschnig, R. M., Rudnick, R. L., McDonough, W. F., Kaufman, A. J., Valley, J. W., Hu, Z., et al. (2016). Compositional Evolution of the Upper Continental Crust through Time, as Constrained by Ancient Glacial Diamictites. *Geochimica Cosmochimica Acta* 186, 316–343. doi:10.1016/j.gca.2016.03.020

Han, T., Fan, H., and Wen, H. (2018). Dwindling Vanadium in Seawater during the Early Cambrian, South China. *Chem. Geol.* 492, 20–29. doi:10.1016/j.chemgeo.2018.05.022

Hoffman, P. F., Abbot, D. S., Ashkenazy, Y., Benn, D. I., Brocks, J. J., Cohen, P. A., et al. (2017a). Snowball Earth Climate Dynamics and Cryogenian Geology-Geobiology. *Sci. Adv.* 3, e1600983. doi:10.1126/sciadv.1600983

Hoffman, P. F. (2016). Cryoconite Pans on Snowball Earth: Supraglacial Oases for Cryogenian Eukaryotes? *Geobiology* 14, 531–542. doi:10.1111/gbi.12191

Hoffman, P. F., Halverson, G. P., Schrag, D. P., Higgins, J. A., Domack, E. W., Macdonald, F. A., et al. (2021). Snowballs in Africa: Sectioning a Long-Lived Neoproterozoic Carbonate Platform and its Bathyal Foreslope (NW Namibia). *Earth Sci. Rev.* 2021, 103616. doi:10.1016/j.earscirev.2021.103616

Hoffman, P. F., Lamothe, K. G., LoBianco, S. J. C., Hodgskiss, M. S. W., Bellefroid, E. J., Johnson, B. W., et al. (2017b). Sedimentary Depocenters on Snowball Earth: Case Studies from the Sturtian Chuos Formation in Northern Namibia. *Geosphere* 13, 811–837. doi:10.1130/ges01457.1

Hoffman, P. F. (2011). Strange Bedfellows: Glacial Diamictite and Cap Carbonate from the Marinoan (635 Ma) Glaciation in Namibia. *Sedimentology* 58, 57–119. doi:10.1111/j.1365-3091.2010.01206.x

Ji, B., Yang, K., Zhu, L., Jiang, Y., Wang, H., Zhou, J., et al. (2015). Aerobic Denitrification: a Review of Important Advances of the Last 30 Years. *Biotechnol. Bioproc E* 20, 643–651. doi:10.1007/s12257-015-0009-0

Johnson, B. W., Drage, N., Spence, J., Hanson, N., El-Sabaawi, R., and Goldblatt, C. (2017a). Measurement of Geologic Nitrogen Using Mass Spectrometry, Colorimetry, and a Newly Adapted Fluorometry Technique. *Solid earth.* 8, 307–318. doi:10.5194/se-8-307-2017

Johnson, B. W., Poulton, S. W., and Goldblatt, C. (2017b). Marine Oxygen Production and Open Water Supported an Active Nitrogen Cycle during the Marinoan Snowball Earth. *Nat. Commun.* 8, 1316. doi:10.1038/s41467-017-01453-z

Kennedy, K., and Eyles, N. (2021). Syn-rift Mass Flow Generated 'tectonofacies' and 'tectonosequences' of the Kingston Peak Formation, Death Valley, California, and Their Bearing on Supposed Neoproterozoic Panglacial Climates. *Sedimentology* 68, 352–381. doi:10.1111/sed.12781

Kopf, S., Davidheiser-Kroll, B., and Kocken, I. (2021). Isoreader: An R Package to Read Stable Isotope Data Files for Reproducible Research. *Joss* 6, 2878. doi:10.21105/joss.02878

Kunzmann, M., Gibson, T. M., Halverson, G. P., Hodgskiss, M. S. W., Bui, T. H., Carozza, D. A., et al. (2017). Iron Isotope Biogeochemistry of Neoproterozoic Marine Shales. *Geochimica Cosmochimica Acta* 209, 85–105. doi:10.1016/j.gca.2017.04.003

Kunzmann, M., Halverson, G. P., Scott, C., Minarik, W. G., and Wing, B. A. (2015). Geochemistry of Neoproterozoic Black Shales from Svalbard: Implications for Oceanic Redox Conditions Spanning Cryogenian Glaciations. *Chem. Geol.* 417, 383–393. doi:10.1016/j.chemgeo.2015.10.022

Lau, K. V., Macdonald, F. A., Maher, K., and Payne, J. L. (2017). Uranium Isotope Evidence for Temporary Ocean Oxygenation in the Aftermath of the Sturtian Snowball Earth. *Earth Planet. Sci. Lett.* 458, 282–292. doi:10.1016/j.epsl.2016.10.043

Lechte, M. A., Wallace, M. W., Hood, A. v. S., Li, W., Jiang, G., Halverson, G. P., et al. (2019). Subglacial Meltwater Supported Aerobic Marine Habitats during Snowball Earth. *Proc. Natl. Acad. Sci. U.S.A.* 116, 25478–25483. doi:10.1073/pnas.1909165116

Li, Y., Wiedenbeck, M., Shcheka, S., and Keppler, H. (2013). Nitrogen Solubility in Upper Mantle Minerals. *Earth Planet. Sci. Lett.* 377-378, 311–323. doi:10.1016/j.epsl.2013.07.013

Link, P. K., and Christie-Blick, N. (2011). Chapter 38 Neoproterozoic Strata of Southeastern Idaho and Utah: Record of Cryogenian Rifting and Glaciation. *Geol. Soc. Lond. Memoirs* 36, 425–436. doi:10.1144/m36.38

Merdith, A. S., Collins, A. S., Williams, S. E., Pisarevsky, S., Foden, J. D., Archibald, D. B., et al. (2017). A Full-Plate Global Reconstruction of the Neoproterozoic. *Gondwana Res.* 50, 84–134. doi:10.1016/j.gr.2017.04.001

Mettam, C., Zerkle, A. L., Claire, M. W., Izon, G., Junium, C. J., and Twitchett, R. J. (2017). High-frequency Fluctuations in Redox Conditions during the Latest Permian Mass Extinction. *Palaeogeogr. Palaeoclimatol. Palaeoecol.* 485, 210–223. doi:10.1016/j.palaeo.2017.06.014

Mitchell, R. N., Gernon, T. M., Cox, G. M., Nordsvan, A. R., Kirscher, U., Xuan, C., et al. (2021). Orbital Forcing of Ice Sheets during Snowball Earth. *Nat. Commun.* 12, 4187–4189. doi:10.1038/s41467-021-24439-4

Morales, L. V., Granger, J., Chang, B. X., Prokopenko, M. G., Plessen, B., Gradinger, R., et al. (2014). Elevated 15N/14N in Particulate Organic Matter, Zooplankton, and Diatom Frustule-Bound Nitrogen in the Ice-Covered Water Column of the Bering Sea Eastern Shelf. *Deep Sea Res. Part II Top. Stud. Oceanogr.* 109, 100–111. doi:10.1016/j.dsr2.2014.05.008

Nowicki, B. L. (1994). The Effect of Temperature, Oxygen, Salinity, and Nutrient Enrichment on Estuarine Denitrification Rates Measured with a Modified Nitrogen Gas Flux Technique. *Estuar. Coast. Shelf Sci.* 38, 137–156. doi:10.1006/ecss.1994.1009

Ojakangas, R. W., and Matsch, C. L. (1980). Upper Precambrian (Eocambrian) Mineral Fork Tillite of Utah: a Continental Glacial and Glaciomarine Sequence. *Geol. Soc. Am. Bull.* 91, 495–501. doi:10.1130/0016-7606(1980)91<495:upemft>2.0.co;2

Peng, Y., Dong, L., Ma, H., Wang, R., Lang, X., Peng, Y., et al. (2020). Surface Ocean Nitrate-Limitation in the Aftermath of Marinoan Snowball Earth: Evidence from the Ediacaran Doushantuo Formation in the Western Margin of the Yangtze Block, South China. *Precambrian Res.* 347, 105846. doi:10.1016/j.precamres.2020.105846

Poulton, S. W., and Canfield, D. E. (2005). Development of a Sequential Extraction Procedure for Iron: Implications for Iron Partitioning in Continentally Derived Particulates. *Chem. Geol.* 214, 209–221. doi:10.1016/j.chemgeo.2004.09.003

Poulton, S. W., and Canfield, D. E. (2011). Ferruginous Conditions: A Dominant Feature of the Ocean through Earth's History. *Elements* 7, 107–112. doi:10.2113/gselements.7.2.107

Poulton, S. W., Fralick, P. W., and Canfield, D. E. (2010). Spatial Variability in Oceanic Redox Structure 1.8 Billion Years Ago. *Nat. Geosci.* 3, 486–490. doi:10.1038/ngeo889

Poulton, S. W., Fralick, P. W., and Canfield, D. E. (2004). The Transition to a Sulphidic Ocean ~ 1.84 Billion Years Ago. *Nature* 431, 173–177. doi:10.1038/nature02912

Poulton, S. W. (2021). *The Iron Speciation Paleoredox Proxy*. Cambridge: Cambridge University Press.

Quan, T. M., van de Schootbrugge, B., Field, M. P., Rosenthal, Y., and Falkowski, P. G. (2008). Nitrogen Isotope and Trace Metal Analyses from the Mingolsheim Core (Germany): Evidence for Redox Variations across the Triassic-Jurassic Boundary. *Glob. Biogeochem. Cycles* 22, a–n. doi:10.1029/2007GB002981

Quan, T. M., Wright, J. D., and Falkowski, P. G. (2013). Co-variation of Nitrogen Isotopes and Redox States through Glacial-Interglacial Cycles in the Black Sea. *Geochimica Cosmochimica Acta* 112, 305–320. doi:10.1016/j.gca.2013.02.029

Raiswell, R., and Canfield, D. E. (1998). Sources of Iron for Pyrite Formation in Marine Sediments. *Am. J. Sci.* 298, 219–245. doi:10.2475/ajs.298.3.219

Richardson, D. J., Berks, B. C., Russell, D. A., Spiro, S., and Taylor, C. J. (2001). Functional, Biochemical and Genetic Diversity of Prokaryotic Nitrate Reductases. *Cell. Mol. Life Sci.* 58, 165–178. doi:10.1007/PL00000845

Sahoo, S. K., Planavsky, N. J., Kendall, B., Wang, X., Shi, X., Scott, C., et al. (2012). Ocean Oxygenation in the Wake of the Marinoan Glaciation. *Nature* 489, 546–549. doi:10.1038/nature11445

Sigman, D. M., DiFiore, P. J., Hain, M. P., Deutsch, C., Wang, Y., Karl, D. M., et al. (2009). The Dual Isotopes of Deep Nitrate as a Constraint on the Cycle and Budget of Oceanic Fixed Nitrogen. *Deep Sea Res. Part I Oceanogr. Res. Pap.* 56, 1419–1439. doi:10.1016/j.dsr.2009.04.007

Sperling, E. A., Wolock, C. J., Morgan, A. S., Gill, B. C., Kunzmann, M., Halverson, G. P., et al. (2015). Statistical Analysis of Iron Geochemical Data Suggests Limited Late Proterozoic Oxygenation. *Nature* 523, 451–454. doi:10.1038/nature14589

Stüeken, E. E., Buick, R., Guy, B. M., and Koehler, M. C. (2015). Isotopic Evidence for Biological Nitrogen Fixation by Molybdenum-Nitrogenase at 3.2 Gyr. *Nature* 520, 666–669. doi:10.1038/nature14180

Stüeken, E. E., Buick, R., and Lyons, T. W. (2019a). Revisiting the Depositional Environment of the Neoproterozoic Callanna Group, South Australia. *Precambrian Res.* 334, 105474. doi:10.1016/j.precamres.2019.105474

Stüeken, E. E., Kipp, M. A., Koehler, M. C., and Buick, R. (2016b). The Evolution of Earth's Biogeochemical Nitrogen Cycle. *Earth-Science Rev.* 160, 220–239. doi:10.1016/j.earscirev.2016.07.007

Stüeken, E. E., Kipp, M. A., Koehler, M. C., Schwieterman, E. W., Johnson, B., and Buick, R. (2016a). Modeling pN2 through Geological Time: Implications for Planetary Climates and Atmospheric Biosignatures. *Astrobiology* 16, 949–963. doi:10.1089/ast.2016.1537

Stüeken, E. E., Martinez, A., Love, G., Olsen, P. E., Bates, S., and Lyons, T. W. (2019b). Effects of pH on Redox Proxies in a Jurassic Rift Lake: Implications for Interpreting Environmental Records in Deep Time. *Geochimica Cosmochimica Acta* 252, 240–267. doi:10.1016/j.gca.2019.03.014

Tesdal, J.-E., Galbraith, E. D., and Kienast, M. (2013). Nitrogen Isotopes in Bulk Marine Sediment: Linking Seafloor Observations with Subseafloor Records. *Biogeosciences* 10, 101–118. doi:10.5194/bg-10-101-2013

Thomazo, C., Ader, M., and Philippot, P. (2011). Extreme 15N-Enrichments in 2.72-Gyr-Old Sediments: Evidence for a Turning Point in the Nitrogen Cycle. *Geobiology* 9, 107–120. doi:10.1111/j.1472-4669.2011.00271.x

Tribovillard, N., Algeo, T. J., Lyons, T., and Riboulleau, A. (2006). Trace Metals as Paleoredox and Paleoproductivity Proxies: an Update. *Chem. Geol.* 232, 12–32. doi:10.1016/j.chemgeo.2006.02.012

Veraart, A. J., De Klein, J. J. M., and Scheffer, M. (2011). Warming Can Boost Denitrification Disproportionally Due to Altered Oxygen Dynamics. *PLoS One* 6, e18508. doi:10.1371/journal.pone.0018508

Wang, W., Guan, C., Zhou, C., Peng, Y., Pratt, L. M., Chen, X., et al. (2017). Integrated Carbon, Sulfur, and Nitrogen Isotope Chemostratigraphy of the Ediacaran Lantian Formation in South China: Spatial Gradient, Ocean Redox Oscillation, and Fossil Distribution. *Geobiology* 15, 552–571. doi:10.1111/gbi.12226

Wei, G.-Y., Planavsky, N. J., He, T., Zhang, F., Stockey, R. G., Cole, D. B., et al. (2021). Global Marine Redox Evolution from the Late Neoproterozoic to the Early Paleozoic Constrained by the Integration of Mo and U Isotope Records. *Earth-Science Rev.* 214, 103506. doi:10.1016/j.earscirev.2021.103506

Yonkee, W. A., Dehler, C. D., Link, P. K., Balgord, E. A., Keeley, J. A., Hayes, D. S., et al. (2014). Tectono-stratigraphic Framework of Neoproterozoic to Cambrian Strata, West-Central U.S.: Protracted Rifting, Glaciation, and Evolution of the North American Cordilleran Margin. *Earth-Science Rev.* 136, 59–95. doi:10.1016/j.earscirev.2014.05.004

Young, G. M. (2002). Geochemical Investigation of a Neoproterozoic Glacial Unit: the Mineral Fork Formation in the Wasatch Range, Utah. *Geol. Soc. Am. Bull.* 114, 387–399. doi:10.1130/0016-7606(2002)114<0387:gioang>2.0.co;2

Zerkle, A. L., and Mikhail, S. (2017). The Geobiological Nitrogen Cycle: From Microbes to the Mantle. *Geobiology* 15, 343–352. doi:10.1111/gbi.12228

Zerkle, A. L., Poulton, S. W., Newton, R. J., Mettam, C., Claire, M. W., Bekker, A., et al. (2017). Onset of the Aerobic Nitrogen Cycle during the Great Oxidation Event. *Nature* 542, 465–467. doi:10.1038/nature20826

Zhang, X., Sigman, D. M., Morel, F. M. M., and Kraepiel, A. M. L. (2014). Nitrogen Isotope Fractionation by Alternative Nitrogenases and Past Ocean Anoxia. *Proc. Natl. Acad. Sci. U.S.A.* 111, 4782–4787. doi:10.1073/pnas.1402976111

Conflict of Interest: The authors declare that the research was conducted in the absence of any commercial or financial relationships that could be construed as a potential conflict of interest.

Publisher's Note: All claims expressed in this article are solely those of the authors and do not necessarily represent those of their affiliated organizations, or those of the publisher, the editors and the reviewers. Any product that may be evaluated in this article, or claim that may be made by its manufacturer, is not guaranteed or endorsed by the publisher.The standard for N isotopes is atmospheric N_2, which is set to $0^0/_{00}$ by definition.